International Journal of Rock Mechanics and Mining Sciences 121 (2019) 104049

Contents lists available at ScienceDirect

International Journal of Rock Mechanics and Mining Sciences

journal homepage: www.elsevier.com/locate/ijrmms

Investigation of longwall headgate stress distribution with an emphasis on pillar behavior

Sankhaneel Sinha*, Gabriel Walton

Colorado School of Mines, Golden, CO, USA

ARTICLE INFO

Keywords:
Longwall mining
Stress redistribution
Global stress
Abutment angle
Numerical modeling

ABSTRACT

This study uses an extensive suite of borehole pressure cell (BPC) data from a US longwall mine to better characterize the global stress redistribution process during mining. A new methodology employing the Bieniawksi's strength gradient equation was used for converting the BPC measurements into rock pressure. It was observed that the Bieniawksi gradient equation underestimates coal strength for points located deeper into the pillar. Comparisons with previous empirical and analytical equations are also presented for different stages of longwall loading. Very low front abutment load in comparison to the side abutment load was observed, along with a low abutment angle for this mine. This abutment angle value was verified from stress measurements made within the solid coal face ahead of the advancing panel. Some other atypical trends were noted during data analyses, such as a monotonic drop in stress from the panel edge within the coal face; these trends were explained using an elastic FLAC^{3D} model. Finally, the load distribution in a pillar is presented in three-dimensions using interpolated bar graphs for different locations of the longwall face.

1. Introduction

With technological advances in the last few decades, longwall mining has grown to be the most productive coal mining technique in the United States. In contrast to the room and pillar mining method, longwall mining involves the complete extraction of the coal block, often termed as the 'panel', allowing the roof to collapse in the mined-out area.[1,2] Since these extracted areas are often hundreds of meters wide, substantial redistribution of stresses occurs within adjacent chain pillars with passage of the longwall face.[3] Broadly speaking, the loads applied to longwall chain pillars can be divided into two parts[3]: (a) Development load: This is the load associated with the development of the entries and can be estimated using the tributary area method; (b) Abutment load: This is the load that is associated with the extraction of the panel and is unique to the retreat mining nature of longwall. The abutment load can be further categorized into two load levels based on the location of the longwall face relative to the pillar in question. The abutment load when the face is at a position of 0 m relative to the pillar (i.e. face at the pillar) is called the 'front abutment load' and the abutment load long after the face has gone past the pillar is termed as 'side abutment load'.

The load redistribution process in chain pillars during longwall advance has been a topic of research since the 1970s.[2,4,5] Since then, numerous authors have tried to quantify mining-induced stress magnitudes using field measurements,[3,6–8] analytical approaches[9] and numerical models.[10–13] A proper understanding of the stress distribution mechanism at a global scale and its effect on the local behavior of chain pillars is critical in designing ground control systems for longwall gate entries. The large stresses that are typical in longwall mines can lead to pillar failure or violent rib bursts[14]; an example of pillar rib degradation associated with headgate side abutment load is shown in Fig. 1.

Analytical approaches for predicting stress levels in longwall chain pillars rely on assumptions about the internal damage mechanics of coal pillars. The most popular and well known method by Carr and Wilson[9] uses a stress balance approach to distribute the abutment stress onto the chain pillar following an exponential decay function. The loss of load carrying capacity of the pillar rib and subsequent transfer of stress deeper into the pillar is controlled by the 'Limit and Roadway Stability' and the 'Ultimate Limit' concept introduced by Wilson.[5] However, as indicated by Mark,[3] the sequence of damage and load redistribution process assumed by Wilson[5] is not that of a progressive failure, but a process where the initial yield zone does not expand until a certain magnitude of average stress builds up in the pillar core. These solutions also require input parameters that are hard to determine (for example, uniaxial compressive strength of failed coal and friction angle of coal at

* Corresponding author. Colorado School of Mines, 1516 Illinois Street, Golden, CO, 80401, USA.
E-mail address: sankhaneelsinha@mymail.mines.edu (S. Sinha).

https://doi.org/10.1016/j.ijrmms.2019.06.008
Received 5 December 2018; Received in revised form 15 March 2019; Accepted 2 June 2019
Available online 05 August 2019
1365-1609/

Fig. 1. Extensive rib damage in an underground coal mine in the Western US.

the field scale rather than the laboratory scale). More recently, Rezaei et al.[15,16] used energetic considerations[17] to compute the stress concentration factors on longwall chain pillars. While the approach is novel, it considers the coal mass as an elastic isotropic material, meaning that any local stress redistribution due to damage is not accounted for within this analytical framework.

With advent of advanced modeling techniques, numerous studies have been undertaken to understand the longwall gateroad loading process. Esterhuizen et al.[18] used a continuum-based model to simulate the abutment stresses in chain pillars for three different case studies. Yastili and Unver[19] attempted to model a longwall mine in Turkey that employed top-coal caving behind the face. Zhang et al.[20] utilized FLAC^{3D} to study the stress changes in longwall pillars with various sizes. In all these studies, the authors unanimously highlight the difficulty of modeling gob - the gob undergoing continued consolidation with increase in load. This is further exacerbated by our limited understanding of coal mass behavior and how it is affected by the orientation and frequency of cleats. With all this in mind, it is clear that numerical modeling presents several challenges when it comes to studying the global stress transfer process in longwall mines.

A valuable alternative to the previously described methods is to use field data to empirically characterize the load redistribution process. The advantage of this method is its ability to account for the complex components of the system (and their interaction) without having to consider them explicitly. The first such systematic study was conducted by Mark,[3] who developed mathematical relationships for describing the abutment loads (front and side abutment load) and their distributions over the chain pillars; all mines considered in this study were located in the eastern US. Contrary to Carr and Wilson,[9] Mark[3] found an inverse square relationship to best describe the decay of abutment stress in the pillars. Since then, numerous studies have employed borehole pressure cell (BPC) measurements[21–24] and tomography[25–28] to further our understanding of load transfer in longwall panels.

In this study, data from 44 BPCs are utilized for interpreting the load transfer mechanism in context of previously conducted analytical and empirical studies.[3,9,29] The BPCs were installed by mine personnel and a contractor in two adjacent chain pillars in a Western US longwall panel. Stress measurements commenced 245 m in front of (outby) the face and continued until the face was 400 m ahead of (outby) the instrumented pillars. The spatial distribution of the BPCs within the chain pillars provided detailed information on the local pillar response as the global stress state in the ground was perturbed by the retreat of the longwall face. In order to ensure anonymity, the mine under consideration is referred to as 'Mine A'.

2. Site description and instrument locations

2.1. Regional and site geology

Mine A is located in an asymmetric basin formed during the Laramide Orogeny (occurred approximately 75 to 45 million years ago). The entire basin covers an area of about 17,000 km^2 and is about 225 kms wide and 320 kms long. It is bounded in the west, north and east by a steeply dipping monocline and along the south by a zone of uplift. The formation housing the coal bed is of Upper Cretaceous age and was deposited as interbedded marine and non-marine strata during transgression and regression cycles. It is composed mainly of coal, mudstones, carbonaceous mudstones, siltstones and sandstones.

Multiple coal seams are present within this host formation. At Mine A, the seam dips at a very shallow angle ($< 3^{\circ}$) towards east-northeast and ranges in thickness from 2.5 to 4 m. More broadly, the seam exhibits a gently plunging synclinal structure with its axis aligned along the E-W direction. The majority of the immediate roof in the mine is composed of carbonaceous mudstones that slake and degrade in the presence of water.

2.2. Site description

The average depth of mining at the instrumented location is 250 m below ground surface. The particular panel under consideration has a width of 306 m. The adjacent development entries are about 6 m wide and 2.8 m high. Primary roof support consists of 22 mm diameter, 1.83 m long, grade 60 fully grouted rebars, spaced at 0.9–1.3 m across the entry and 1–1.4 m along the entry axis. Roof trusses are also installed on cycle in some areas, but are normally considered as secondary means of ground support. Table 1 lists the unconfined compressive strengths and Young's modulus derived from laboratory testing on standard rock samples[30] and the mean Q for different lithologies at the mine.

2.3. Instrumentation details

Sixteen arrays of BPCs were installed in two chain pillars and the solid coal of the adjacent panel between X-Cut 10 and 11 at Mine A. Fig. 2 shows the location of each linear instrumentation array and the distance of each BPC (marked by red dots) along its length. A hydraulic pump was used to pressurize each cell to a pressure of about 5.5 MPa. All BPC gauges and lines were secured to roof and rib mesh to protect them from potential hazards. BPC arrays 1 and 3 were installed at an angle of 30.7° to the rib in order to ensure adequate space for erecting permanent seals between Entry 2 and 3. Similarly, BPC arrays 2 and 4 were installed at an angle of 14.7° outby of the future seal location for clearance.

To record the data generated by the forty-four BPCs, two Roctest dataloggers were securely mounted directly above X-Cut 11 on the ground surface. The fiber optic cables were routed via existing 18 cm boreholes in the panel. Out of the forty-four BPCs, forty-three of them were operational throughout the monitoring period with the exception of the BPC in array 8 located closest to the rib surface. When installing the BPC arrays, care was taken to set them to within a very close margin of the design depth. Stress measurements commenced when the face

Table 1
Geomechanical characterization for different strata at Mine A.

Lithology	Unconfined Compressive Strength (MPa)	Young's Modulus (GPa)	Q values
Coal	5.4–11.4	2.3–7.8	13–23.7
Mudstones	1.3–5.5	0.78–1.76	5.5–9.4
Siltstones	5.1–51.2	6.4–18.6	11.3–18.2
Sandstones	29.9–50.3	8.8–20.1	23.4–51.7

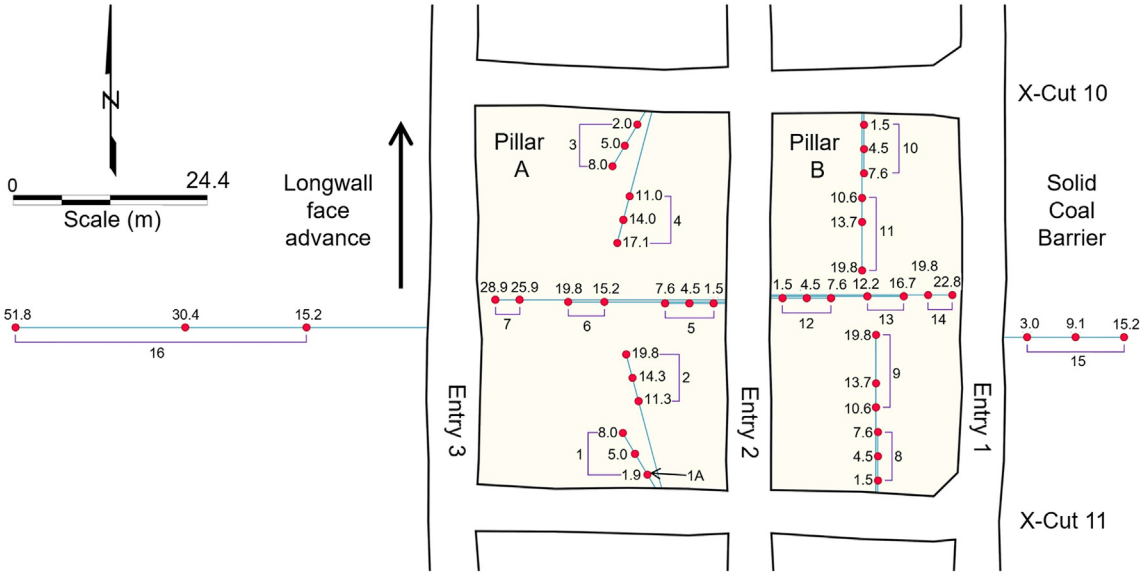

Fig. 2. Location of BPCs in the chain pillars. All units are in meters.

was 245 m away and continued for six months until the face was 400 m outby of X-Cut 10.

3. Existing models for stress transfer in longwall mines

3.1. Abutment angle model and load transfer distance

The most common approach for estimating abutment stress is through the concept of 'abutment angle' (β), which defines the proportion of overburden load above gob that is transferred to the chain pillars (Fig. 3). While the term 'abutment angle' has been also called 'negative angle of draw' by Choi and McCain[10] and 'shear angle' by King and Whittaker,[4] its relationship to subsidence profiles is not straightforward.[31] Mark[3] considered it to be a mathematical approximation of physical reality rather than a true measurable characteristic of the gob. For subcritical panels, the abutment angle is related to the side abutment load L_{SS} as:

$$L_{ss} = \gamma\left(\frac{HP}{2} - \frac{P^2}{8\tan\beta}\right) \quad (1)$$

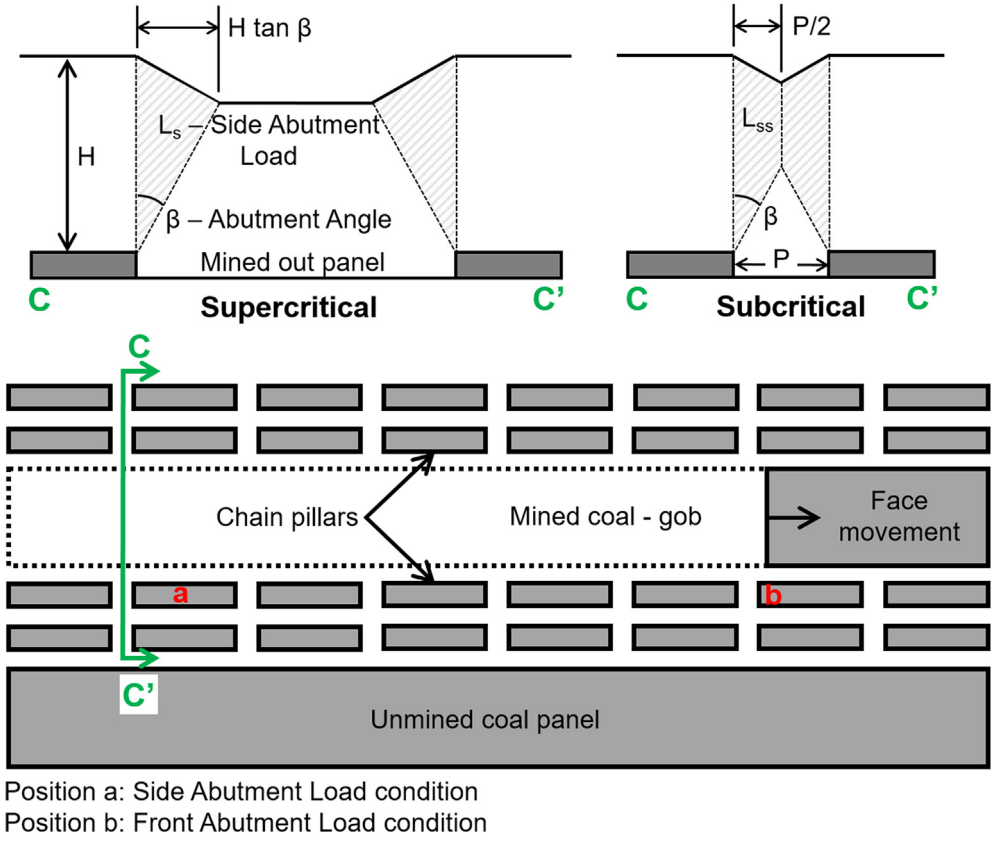

Fig. 3. Abutment angle concept (after[10]) with the front and side abutment load conditions (after[32]).

where H is the depth of cover, P is the panel width, γ is the unit weight of overburden, and β is the abutment angle. For critical and supercritical panels, the equation for side abutment load (L_s) is as follows:

$$L_s = H^2 \tan\beta \left(\gamma/2\right) \quad (2)$$

The abutment load, in general, is characterized by the front abutment and the side abutment load. The side abutment load can be easily computed in two dimensions using Eqs. (1) or (2). The front abutment load, on the other hand, is difficult to quantify mathematically, since the stresses are unequally distributed in three dimensions within the solid coal ahead (outby) of the longwall face, the chain pillars and the gob depending on the effective stiffness of each of these components of the mine system. While numerical modeling can be used to study this process, selection of proper constitutive models to represent coal mass and gob behavior may be difficult. This is because of our lack of complete understanding of how coal masses and gob material behave under increasing levels of load and how this behavior can be appropriately represented using material constitutive relationships.

Empirical characterization on the basis of field measurements is often useful when dealing with problems that cannot be analyzed using basic mathematics. Mark[3] found from previous field studies that the front abutment load is considerably lower than the side abutment load, and that the two can be related as $L_f = F(L_s)$, where F is the 'front abutment factor', with a value less than 1. From a physical standpoint this is intuitive, since a significant portion of the front abutment load is carried by the solid coal face. Further analyses of the front abutment loads by Mark[3] revealed that F ranges from 0.38 to 0.68 with 0.5 being the mean value. He also concluded $\beta = 21^\circ$ to be a conservative estimate of abutment angle for US coal mining conditions. Subsequent studies, however, have found β to decrease with increasing mining depth.[33,34]

The abutment loads generated by the retreat of a longwall face can only be detected up to a finite distance from the edge of the panel. Peng and Chiang[2] analyzed field stress measurements to develop a relationship between the load transfer distance (LTD) and mining depth (H), which is given by:

$$LTD\ (m) = 5.13\sqrt{H\ (m)} \quad (3)$$

More recently, Larson et al.[35] proposed a negative exponential relationship based on a large database of LTD observations from various mines. Field measurements made by Larson et al.[35] indicated a much larger LTD in comparison to that predicted by Eq (3). An important conclusion drawn in this study was that the relationship between LTD and H is non-unique and is dependent on the overburden geology. As a result, a single equation might not be applicable to every geo-mining condition.

3.2. Abutment load distribution

The distribution of the abutment load on longwall chain pillars is non-uniform in nature. From stress measurements made at five mines, Mark[3] proposed a square decay relationship with distance from panel edge, given by:

$$\sigma_{abutment} = \frac{L_s}{D^3}(D - x)^2 \quad (4)$$

where $\sigma_{abutment}$ is the abutment stress level at a given position, L_s is the total side abutment load, D is the LTD (defined in Eq. 3) and x is the distance from the panel edge. An alternate analytical relationship was proposed by Wilson[29]:

$$\sigma_{abutment} = (\hat{\sigma} - q)\, e^{\left(\frac{-x}{C}\right)} \quad (5)$$

where $\hat{\sigma}$ is the peak abutment stress, q is the cover load, x is the distance from the rib into the solid coal, and y is a constant with units of distance. In absence of any yield zone, C can be estimated as follows[3]:

$$C = \frac{L_s}{\hat{\sigma} - q} \quad (6)$$

3.3. Depth of yield in coal pillars

To predict the depth of failure in pillars, Wilson[29] proposed two analytical equations considering yield in the coal seam only and yield in the roof, floor and coal seam. The analytical equations are expressed as:

$$\text{Yield in roof, floor and coal: } x_b = \frac{M}{2}\left[\left(\frac{q}{p + p'}\right)^{1/(k-1)} - 1\right] \quad (7)$$

$$\text{Yield in coal only: } x_b = \frac{M}{F}\ln\left(\frac{q}{p + p'}\right) \quad (8)$$

where, x_b is the depth of yield, M is the height of the pillar, q is the vertical stress associated with rock cover, k is the triaxial stress factor, p is the restraint on the boundary (expressed as a stress), p' is the uniaxial strength of fractured coal, and, F is defined as follows:

$$F = \frac{k-1}{k^{1/2}} + \left(\frac{k-1}{k^{\frac{1}{2}}}\right)^2 tan^{-1}\left(k^{\frac{1}{2}}\right) \quad (9)$$

4. Results

4.1. Expected stress redistribution and stress cell data

In this paper, measurements from the forty-four Borehole Pressure Cells are critically analyzed in context of previously proposed models[3,9,29] for stress redistribution during longwall mining to gain a better understanding of this process. The chain pillar closest to the panel is termed as 'Pillar A' while the one closer to the solid coal barrier is termed as 'Pillar B'. Since stresses are non-uniformly distributed within pillars,[26,36] a sufficient spread of measurement points along the width of a pillar is required to accurately estimate the average stress. In this case, seven BPCs are located along the width of Pillar A and B (refer to Fig. 2), which made it possible to compute the average stress magnitudes with reasonable confidence. Fig. 4c shows the average stress change in Pillar A and B as a function of the face location. To compute these stresses, the areas under the stress profiles for Pillar A and B were first determined using Surveyor's formula[37] and then divided by the respective pillar widths. The corresponding equation for Pillar A is as follows:

$$\sigma_{A,avg} = \frac{0.5\left|\sum_{i=1}^{n-1} x_i\sigma_{i+1} - \sum_{i=1}^{n-1} x_{i+1}\sigma_i + x_n\sigma_1 - x_1\sigma_n\right|}{Width\ of\ Pillar\ A} \quad (10)$$

where $\sigma_{A,avg}$ is the average stress for pillar A, x_i is the distance of different datapoints from panel edge, and, σ_i is the measured stress magnitude at the corresponding datapoints.

Stress in Pillar A started to increase rapidly when the face was 30 m behind (inby) the pillar (the leftmost point in Fig. 4c) and continued to rise with further face movement. Interestingly, just after the passage of the longwall face, a temporary loss of load was detected in Pillar A (Fig. 4a). Such an observation was also made in Mark[3] while analyzing the stress measurements from Kitt Mine in West Virginia. The explanation proposed by Mark[3] is the release of stress that occurs due to caving behind (inby) the face. With the approach of the longwall face, a cantilever is formed in the roof that is supported by the solid coal and the chain pillars. As the face advances, the cantilever breaks, temporarily relieving the load in the chain pillar. Finally, as the face moves further and further away, additional deflection of the roof occurs which increases the stress in the pillars.

The stress measurements shown in Fig. 4c only represent the stress change recorded by the BPC and not the actual stress change in the

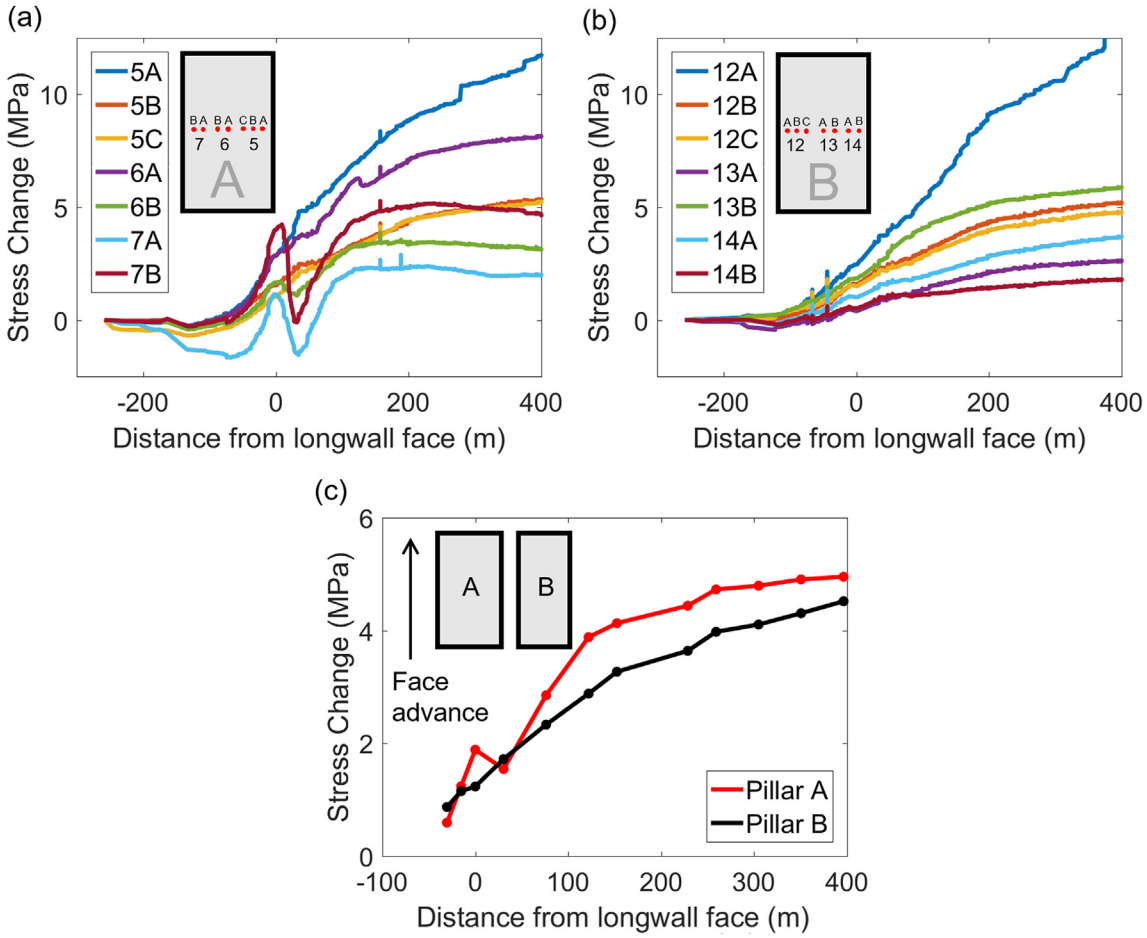

Fig. 4. (a) Stress change profile for BPC 5A-7B, (b) Stress change profile for BPC 12A-14B (c) Change in average BPC stress with face location for Pillar A and B.

surrounding rock. Generally, the two stress magnitudes can be related by a constant; the exact value of this constant is dependent on the instrument used, host rock elastic properties, pre-stress applied during installation, etc.[33,38–41] Since it was not possible to gather these details to determine the conversion factor, a different approach was undertaken in this study (similar to the approach used by Tulu and Heasley[33]).

4.2. Conversion of BPC measurements into rock stress

Mark and Iannacchione[21] estimated the stress gradient at ultimate load for different pillar strength formulas. In the same study, a comparison was made between yield stresses measured in the field from six different mines and empirical equations. It was found that the Bieniawski[1] stress gradient provides the best estimate of the yield stresses within a pillar, although it diverges from the average field-measured curve for points located deeper in the pillar. The corresponding equation is as follows[21]:

$$\sigma_v(x) = S_1\left(0.64 + 2.16\,\frac{x}{h}\right) \tag{11}$$

where S_1 is the in-situ coal uniaxial strength, $\sigma_v(x)$ is the coal stress at a distance x from the pillar edge, and h is the height of the pillar.

From the measured stress profiles at Mine A (see Fig. 4a), it was observed that the three BPC closest to the rib (7B, 7A and 6B) yielded at stress levels of 5.15 MPa, 2.33 MPa and 3.39 MPa when the face was 228 m outby. Plugging the relevant x values into Eq. (11), with a mining height of 2.80 m and S_1 of 6.2 MPa,[42] gives $\sigma_{v,7B}$ = 16.0 MPa, $\sigma_{v,7A}$ = 30.4 MPa and $\sigma_{v,6B}$ = 59.5 MPa. Since the BPC exhibited a continued drop in stress beyond this point, it can be reasonably assumed that the coal strength was attained at this location. The conversion factor (CF) could then be calculated as the ratio of the strength obtained from Eq. (11) to the failure stress (development stress using tributary area method + stress measured by BPC), resulting in three possible conversion factors: CF_{7B} = 1.21, CF_{7A} = 2.90 and CF_{6B} = 5.19. The discrepancy between conversion factors may, in part, be due to the fact the tributary area method neglects variations in stress within individual pillars. Only CF_{7B} was utilized for adjusting the BPC measurements for subsequent analyses. The choice of conversion factor is further justified in Section 4.5 through an inspection of BPC Array 16 stress data.

4.3. Calculation of abutment loads and abutment angle

With the BPC measurements converted into actual rock stress values, the next task was to determine the front abutment and side abutment loads at Mine A. As defined earlier, the calculation for front abutment load is performed using the stress data corresponding to a face location of 0. With further face advance, the average stress in Pillar A and B rises (see Fig. 4c) and then flattens out at a distance of around 260 m from face. While the 260 m face location could be used to estimate the side abutment load, the 400 m location was chosen (as the final data location) for the purposes of side abutment load assessment. The authors would like to point out that there was a 21.6% and 36.3% increase in average stress for Pillar A and B respectively between face locations 115 m and 400 m. In the work by Mark,[3] due to extensive instrument damage, the side abutment calculation was performed at a face location of 115 m (outby). As a result, there may have been a

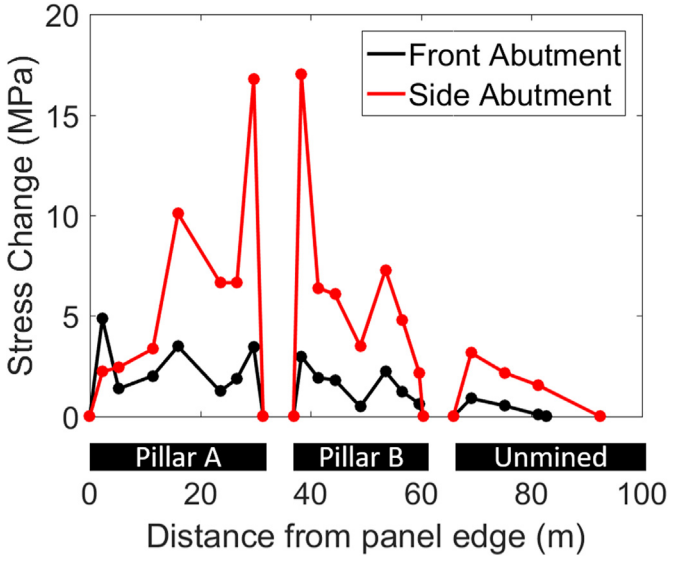

Fig. 5. Stress distribution in Pillar A, Pillar B and solid coal for front loading and side loading condition.

significant underestimation of the side abutment loads in that study.

Fig. 5 shows the stress distribution in Pillars A and B and the adjacent unmined coal for longwall face locations at 0 m outby (front abutment loading) and 400 m outby (side abutment loading). Two important observations can be readily made: (a) there is yield and subsequent loss of load carrying capacity in the first 5 m of the rib between the front and side abutment loading conditions; (b) the proportion of load carried by the unmined coal and LTD increases as the longwall face advances. The two observations can be explained by a progressive damage mechanism where a gradual widening of the fractured rib transfers the load away from the panel edge. It is therefore evident that calculation of the side and front abutment loads requires a proper consideration of load carried by the unmined coal. It should be noted that the right-most datapoint in Fig. 5 was obtained by fitting a straight line to the three stress measurement points in the unmined pillar. The error incurred by using a linear fit instead of an exponential decay or inverse square function is relatively small and can be neglected for practical purposes.

The methodology followed for calculating the front and side abutment load is similar to what was proposed by Mark.[3] The front abutment load per unit length of the entry (L_f), in terms of the average pillar stress, can be represented as:

$$L_f = \frac{\sigma_{A,f} Ar_A + \sigma_{B,f} Ar_B + \sigma_{unmined,s} Ar_{unmined}}{C} \quad (12)$$

where $\sigma_{A,f}$, $\sigma_{B,f}$ and $\sigma_{unmined,f}$ are the average stresses in Pillars A and B and the unmined coal when the face was at 0 m, respectively; Ar_A, Ar_B and $Ar_{unmined}$ are the areas of Pillars A and B and the unmined coal (only the loaded portion of the unmined solid coal was considered in the calculation), and C is the X-cut spacing.

The side abutment load, similarly, can be computed using the following equation:

$$L_s = \frac{\sigma_{A,s} Ar_A + \sigma_{B,s} Ar_B + \sigma_{unmined,s} Ar_{unmined}}{C} \quad (13)$$

where, $\sigma_{A,s}$, $\sigma_{B,s}$ and $\sigma_{unmined,s}$ are the average stresses in Pillars A and B and the unmined coal when the face was 400 m outby, respectively. The respective data-derived input parameters for Eqs. (12) and (13) are listed in Table 2. In order to emphasize the need to include the load borne by the unmined solid coal in front and side abutment load calculations, two independent analyses were conducted. Table 3 presents the front abutment load, side abutment load, abutment angles and the front abutment factors from these analyses. The abutment angle was calculated by equating the side abutment load to Eq. (2) for super-critical panels – for Mine A, the ratio of the depth to the length of panel is 306/252 = 1.21, which is more than the critical value given by Wilson[5] and Agioutantis and Karmis.[43] A unit weight (γ) of 25 kN/m^3 was also considered for this calculation.[3,15,44,45]

Table 2
Input parameters for calculating the front and side abutment loads.

Input parameters	Values (using CF_{7B})	
	Front Abutment	Side Abutment
σ_A(MPa)	2.27	6.11
σ_B (MPa)	1.49	6.09
$\sigma_{unmined}$ (MPa)	0.16	1.54
Ar_A (m^2)	1489	1489
Ar_B (m^2)	1128	1128
$Ar_{unmined}$ (m^2)	796	1260
C (m)	53	53

The front abutment factors (F) obtained are well below the typically value of 0.5 that is commonly applied in the mining industry. With this is mind, chain pillars designed considering $F = 0.5$ would be conservative in nature at Mine A, with the only downside being leaving more coal unmined in the pillars. The F factor has been found to be highly variable and mine specific[24]; a conservative value, therefore, is better suited for preliminary pillar design. Such a low value of F is not an artifact of the choice of conversion factor since its effect is nullified when taking the ratio between the front and side abutment loads.

A comparison of the results with and without consideration of the load on the unmined solid coal revealed a negligible effect on the front abutment load calculation and an 11% error in the side abutment load. The abutment angle also decreased by 1.2° when the load on the unmined coal was ignored. This agrees well with a 2.2° increase in abutment angle reported by Mark[3] when the assumed stress in the solid coal barrier in Kitt mine, WV, was incorporated into the calculation.

4.4. Distribution of abutment loads

4.4.1. Front abutment load

Seven datapoints were available for each chain pillar and three datapoints for the solid unmined coal along the pillar mid-point cross-section. Therefore, the average front abutment stress between every two adjacent datapoints could be computed. The area enclosed by the datapoints was first determined by the Surveyor's formula[37] and then divided by the distance between them. The average stress obtained was then assigned a position at the center of the measurement point pair. Fig. 6 shows the inverse square and the exponential decay fits to the average stress values calculated using this approach. The equation for determiningσ[29] has not been used here, as it assumes the abutment to have reached the peak stress level. It was verified from the BPC measurements that none of the datapoints yielded under the front abutment load. The Wilson[29] equation, therefore, is utilized here purely to test its capability in capturing the trend of the field stress data.

It was possible to fit the curves directly to the BPC measurements, but the approach of averaging adjacent datapoints is more consistent with how the decay equation was developed.[3] Another advantage of this approach is its ability to limit the effect of excavation induced stress concentrations around the edges of the pillar.

Both equations appear to fit the stress data fairly well, with Mark's[3] decay function exhibiting a slightly higher R^2 value in comparison to Wilson's[29] decay function. The L_f (instead of L_s, since the front abutment load is being analyzed here) served as an input parameter for Wilson's[29] equation, and was determined through a least-square curve fitting process for Mark's[3] equation. The best-fit value of L_f was found to be 98.4 MN/m which is within 0.5% of the front abutment load

Table 3
Front, side abutment load, front abutment factor and abutment angle for Mine A.

Case	Front abutment (MN/m)	Side abutment (MN/m)	F	β (deg)
Considering load on unmined coal (CF_{7B})	97.9	337.9	0.29	11.5
Not considering load on unmined coal (CF_{7B})	95.5	301.3	0.32	10.3

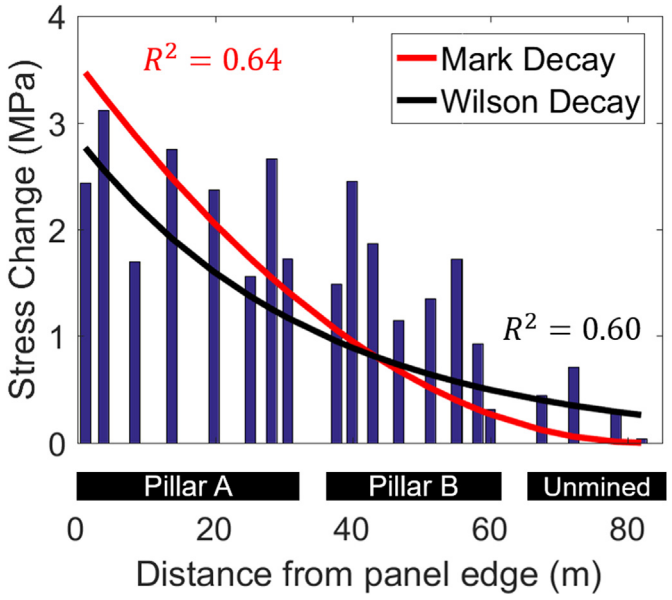

Fig. 6. Inverse square and exponential decay fit to average front abutment stress across the pillars.

computed directly from the stress data. The trend of the two equations in Fig. 6 indicates some differences – Wilson's[29] equation predicts a lower peak abutment stress and better captures the stress levels in the unmined coal, but predicts an infinite LTD. Conversely, Mark's[3] equation predicts a higher peak abutment stress and underestimates the load on unmined coal pillars, but assumes the stress change to terminate at the LTD.

4.4.2. Side abutment load and yield depth

As the longwall face advanced beyond the monitored pillars, an increase in stress was observed across the two chain pillars and in the solid unmined coal of the adjacent panel. The load continued to increase until the face reached 228 m outby, at which point the stresses in BPC Array 7 and instrument 6B started to drop (Fig. 7). The loss in load carrying capacity was compensated by an increase in the BPC stress levels recorded deeper into the pillars. Since the aforementioned BPCs showed a monotonic decrease in stress levels, it can be reasonably inferred that the first 13.7 m (halfway between 4th and 5th datapoint in Fig. 7) of the rib has yielded. The extent of rib damage observed in this case is much larger than those reported in previous studies. For comparison, Mark[3] reported 5.3 m of rib damage for a face location of 40 m outby while Colwell[46] found 4 m of rib damage with face at 981 m outby. Note that the extrapolated rightmost datapoint in Fig. 5 for side abutment loading was located 92.4 m from the panel edge. This is 13.5% higher than the LTD calculated from Eq. (3).

The immediate floor in Mine A is composed mostly of soft mudstones, and it is probable that failure occurred in both the host rock and the coal seam. Equation (7) is, therefore, more appropriate for estimating the depth of yield. Plugging in $q = 6.55$ MPa, $p = 0$ MPa (no lateral restraint, considering the worst case scenario), $M = 2.80$ m, $k = 4$ (equivalent to a friction angle of 37°[29]) and $p' = 0.1$ MPa[3] gives a depth of yield equal to 4.24 m. The analytical solution significantly underestimates the depth of yield in this case. This is not surprising, as

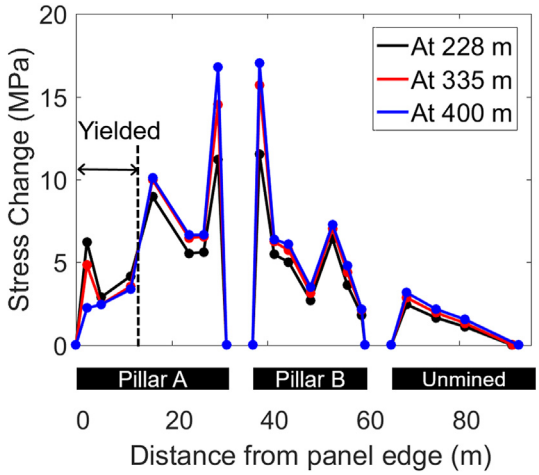

Fig. 7. Stress distribution across the chain pillars and solid unmined coal for different face locations.

the mechanism of fracture initiation and propagation is far more complex than what can be captured using analytical approaches. In addition, the interaction between the host rock and the pillar is unique for any given geo-mining condition, making it difficult to quantify this behavior using a generalized equation.

Wilson's[29] method also assumes the peak stress to occur at the interface between the yield zone and the elastic core. The sudden jump in the stress level 16 m into the pillar (5th datapoint from left in Fig. 7) appears consistent with this assumption. As the stress within the first 11.4 m (4th datapoint from left in Fig. 7) of the rib falls while those beyond 16 m rise with face advance beyond the 228 m outby location, it can be assumed that the edge of the yield zone lies somewhere between 11.4 m and 16 m. In absence of any measurement point within this zone, the center (i.e. 13.7 m) was chosen as the edge of the yielded coal. Based on Wilson's[29] hypothesis then, it could be postulated that the stress level around 13.7 m may be significantly higher than the measured value at 16 m.

In the post-yield stage, Wilson[29] assumed the coal to carry the same elevated stress level as additional load is applied to the pillar. It appears that this assumption is erroneous; significant load transfer occurs from the yield zone to the elastic pillar core and the adjacent chain pillar, even when the pillar has not failed completely.

Mark's[3] decay equation and Wilson's[29] decay equation could only be fitted to the datapoints located 13.7 m or more from the panel edge. This is because stress decay occurs only within the elastic portion of the pillar. The sharp peaks in stress at the edges of the pillar in Fig. 7 are believed to be purely elastic in nature (excavation-adjacent stress concentration) and caused significant distortion in the data-fitting process. In particular, the *Ls* value obtained by fitting Mark's[3] decay equation (considering the sudden peak points) was found to be significantly higher than the Ls computed from BPC data for chain pillars and the solid coal barrier. This is unacceptable, as only a portion of the BPC data (in the elastic portion of the pillar systems) was considered in the data-fitting process, which should have therefore yielded L values lower than the total *L* values for the entire pillar system. In order to eliminate this issue, these two peak stress points were removed from the analysis (but are presented in Fig. 8 as green bars).

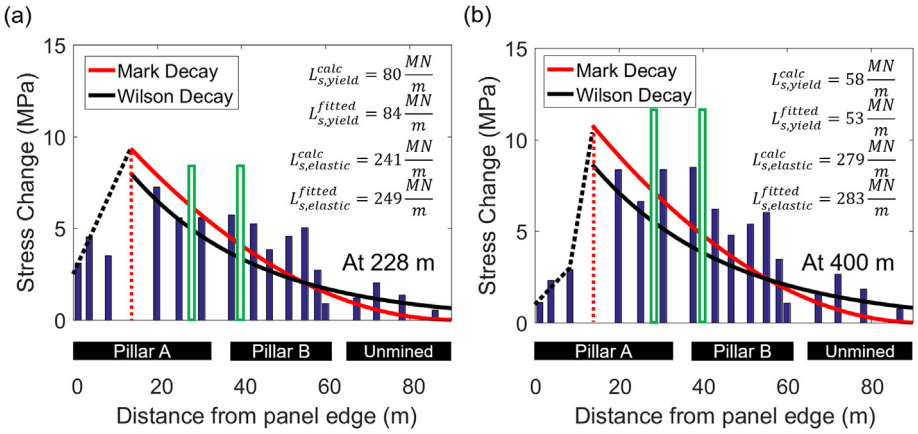

Fig. 8. Curve fit to the datapoints for longwall face locations of (a) 228 m outby, and, (b) 400 m outby. *Ls*, *yieldcalc* and $L^{calc}_{s,elastic}$ indicate the side abutment loads calculated for the yielded and elastic region from the BPC data; $L^{fitted}_{s,yield}$ and $L^{fitted}_{s,elastic}$ indicate the side abutment loads obtained after fitting the respective curves. Data values shown in green were not considered in the curve fitting process. MN/m (Mega-Newton per meter) is the unit of abutment load used in this study. (For interpretation of the references to colour in this figure legend, the reader is referred to the Web version of this article.)

The procedure presented in Section 4.4.1 was followed, whereby the average stress between adjacent datapoints were computed and then assigned to its respective midpoint. This was performed for the datasets corresponding to a longwall face location of 228 m and 400 m outby. Due to lack of any stress measurement between 11.4 m and 16 m within the pillar, the peak stress level at the interface between the elastic core and the yield zone was obtained by setting x = 0 in Mark's[3] decay function at a distance of 13.7 m into the pillar. For the Wilson[29] fit, the portion of the side abutment load carried by the pillar was used to determine 'C'. $\hat{\sigma}$, as obtained from the equation, $\hat{\sigma} = kq + S_1$,[29] for the face location of 228 m led to a poor fit to the data; as a consequence, it was allowed to vary during the fitting process.

Wilson[29] hypothesized an exponential rise in stress levels within the yield zone. Mark,[3] on the other hand, found that a straight line better characterizes the stress gradient from the rib to the elastic core. In this study, an attempt was made to fit both types of curve to the field data. An acceptable fit could not be attained for the exponential curve using constants calculated from Wilson[29] or when using the constants as fit variables. A straight line was deemed to be a simpler and better predictor of the BPC data in the yield zone. To fit the line, an intercept was manually selected on the vertical (stress) axis such that it satisfied both the peak stress level obtained from Mark's[3] decay fit at 13.7 m from the pillar edge as well as the overall trend of the dataset.

Fig. 8a shows the curve fit to the BPC data for the 228 m outby face location. A comparison was made between the proportion of side abutment load carried by the yield zone and the elastic pillar material as obtained from the curve fitting process and from the field data (see Fig. 8a). The ability of the fit in capturing the trend of the BPC data as well as the excellent correspondence in the side abutment load values provides confidence in the data-fitting process.

For the 400 m outby face location, a bi-linear curve was chosen. The fitted curve and the proportion of load carried by the yield zone and elastic pillar material is shown in Fig. 8b. The bi-linear nature of the stress gradient in the yield zone was also observed by the authors in a calibrated FLAC^{3D} model of an Australian longwall mine.[47] The mine is located at a depth of 480 m and has a panel width of approximately 195 m (roadway center to center). Further details on this study can be found in Sinha and Walton.[47] In this case, a model was able to accurately match displacement and stress profiles for different locations of the longwall face. Fig. 9 shows the model predicted stress profiles for three different locations of the longwall face. Given the dissimilarity in the geo-mining condition between Mine A and the Australian mine, only a qualitative comparison was performed here. To that end, normalized stress change profiles were used instead of raw stress change profiles.

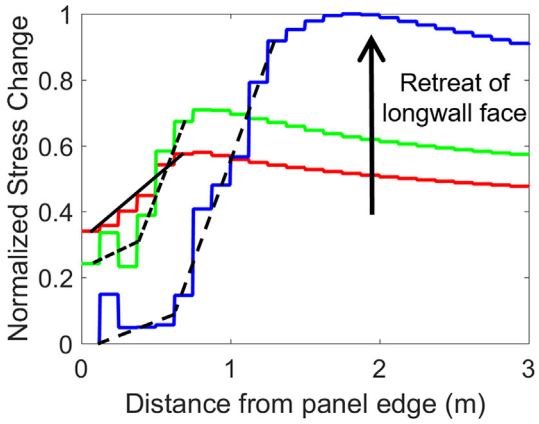

Fig. 9. Normalized stress change versus distance from panel edge from a calibrated numerical model of an Australian longwall case study.

As can be seen from Fig. 9, the stress gradient in the yield zone changes from a linear to a bi-linear shape with the advance of the longwall face. Prior to the formation of a bi-linear shape, the slope of the linear section increases until it reaches a peak value. The skin of the pillar, at this point, attains its residual strength, shedding the excess load deeper into the pillar (shown by the green line). The red and the green line in Fig. 9 can be considered qualitatively similar to the face locations at 228 m and 400 m in Fig. 8. With continued loss of load carrying capacity of the pillar rib, the yield zone finally expands to accommodate the excess stress. It is interesting to note that the slope of the second segment of the bi-linear curve (the portion located closer to the elastic core) remains almost constant during the rib extension process (refer to the red and green curves). Since no BPC measurements were available beyond the 400 m face location, this observation could not be validated at Mine A. During the entire loading process, the peak stress level at the interface between the yield zone and the elastic material was also found to increase in both the numerical model and the field data.

4.5. Stress distribution in coal ahead of (outby) the longwall face

BPC Array 16 was installed in the solid longwall face at distances of 15.2 m, 30.4 m and 51.8 m from the edge of the panel. Fig. 10 shows the stress change profiles as a function of face distance; measurements were terminated when the face was about 7.5 m from the instruments. The BPCs started experiencing load when the face was about 230 m inby the

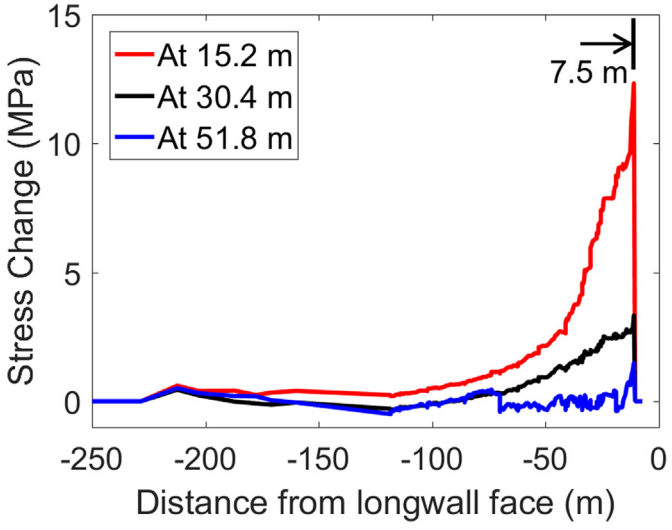

Fig. 10. Stress change profile as measured in the solid longwall face.

instrumented location. Interestingly, BPCs located closer to the chain pillars consistently experienced higher stress levels than those located deeper within the solid coal. Intuitively, one might expect some of the load around the panel edge to be distributed over the chain pillars, resulting in lower stress levels in the solid coal face. That being said, it is unlikely that the data are faulty since that all three BPCs exhibited the same trend.

In the context of the data shown in Fig. 10, some hypotheses were formulated and then tested using a schematic FLAC^{3D} model in Section 5. Here, we argue that when the main roof breaks behind (inby) the longwall face, the region of the gob closest to the chain pillars cannot compact to the same extent as the gob located away from the panel edge. The primary reason is the resistance offered by the chain pillars to reduce the flexure of the roof layers. This means that the effective stiffness of the gob material increases as one moves away from the panel edge. The excess stress near the panel edge (corresponding to the load not carried by the chain pillars) is transferred to the stiffer solid coal and the shield support rather than to the 'soft' gob material. Away from the panel edge, the gob becomes stiffer and can proportionately carry higher loads, reducing the amount of stress channeled to the solid coal face.

At a certain distance behind (inby) the panel face, the gob should be transferring almost the entire load of the overburden to the floor.[48–52] The distance behind the face at which this occurs depends on the type of gob material and the depth of mining. A strong roof material will compact faster and will be able to re-load to the in-situ stress more rapidly than a weak roof material. For Mine A, the behavior of the gob is unknown; however, from Array 7 stress data, it appears that the main roof collapsed about 10 m after the face went past the instruments. This showed up as a drop in the stress levels in Array 7 and 6B and in the average stress for Pillar A (see Fig. 4). Based on this, the authors believe that the relatively low change in stress for the 51.8 m BPC shown in Fig. 10 is related to it being very close to the edge of the abutment influence zone, with the unsupported overburden load from between the 'fully compacted' gob (that is $>$ 10 m behind) and the face being carried primarily by the compacted gob, the shield supports and first 7.5 m of solid coal ahead (outby) of the face. For such effective stress transfer between the three load bearing elements, the gob must have been a material that compacted relatively quickly.

If indeed the 51.8 m BPC was located close to the edge of the abutment influence zone, it could be used to calculate the abutment angle. Tangent inverse of 51.8 m divided by the depth of mining (252 m) gives an abutment angle of 11.6°, which is only 0.1° larger than the value computed using the corrected BPC data. For CF_{7A} and CF_{6B}, Eq. (2) yields $\beta = 26°$ and 41°, corresponding to abutment influence zones of 123 m and 219 m, respectively. Clearly, this is in disagreement with the data presented in Fig. 10. The excellent correspondence obtained with CF_{7B} not only confirms the abutment loading theory but also highlights the robustness of the selected conversion factor. Future studies can use a similar methodology for converting the BPC data to actual rock stress.

For an abutment angle of 21°, the edge of abutment would be located 97 m from the panel edge, in which case the BPC at 51.8 m would have experienced elevated load levels. The side abutment load would also have been overestimated by 89% (using Eq. (2)). A key takeaway from this analysis is that chain pillars designed using a 21° abutment angle (used as default in the Analysis of Longwall Pillar Stability software) may be conservative in nature in some cases.

4.6. Three-dimensional (3D) stress redistribution over chain pillars

In the previous sub-sections, only the stress data along the center of the chain pillars was utilized for estimating the side abutment loads. The purpose was to ignore any three-dimensional stress arching effect to simplify calculations and interpretation. In order to fully utilize the dataset and obtain a better understanding of the stress redistribution process, a three-dimensional analysis was necessary. To that end, 3D bar charts were developed for chain Pillars A and B for four different face locations (see Fig. 11). Stress measurements were available at specific points, which necessitated the use of an interpolation technique to populate stress values throughout the rest of the pillar. As no data points were available around the pillar corners, only a diamond-shaped region could be populated with results from the 'cubic' interpolation scheme in MATLAB.

The distribution of stresses within longwall chain pillars are not only non-uniform but also asymmetric in nature. For chain Pillar A, the peak stress level for all four face locations was situated along the longer axis of the pillar. A probable reason is the three-dimensional arching of the mining-induced stresses over the crosscut that resulted in higher stress concentrations along the shorter edge. The extent of arching is dependent on the surrounding strata, gob characteristics and the integrity of the pillar rib. The 3D effect reduces as one moves towards the center of the pillar, ultimately simplifying to a 2D side loading condition.

With advance of the longwall face, a progressive loss of load carrying capacity was noted in the panel-side rib of Pillar A which channeled the excess stress deeper into the pillar as well as to the adjacent chain pillar (i.e. Pillar B). Rib failure and subsequent load transfer was also noted along the shorter edge of Pillar A (see Fig. 11, parts c and d).

5. Analysis of stress transfer mechanism using a hypothetical continuum model

A half panel model with the geometry of Mine A was developed in FLAC^{3D}[53] (see Fig. 12) with the goal of testing two aspects of the stress transfer mechanism hypothesized above: (a) Is the continued drop in stress from the panel edge (as indicated in Fig. 10) due to the differential compaction of gob? (b) Can the unsupported overburden that extends between the uncompacted gob and the shield support be carried by different load-carrying areas such that no stress change is registered 10 m into the solid coal face (i.e. at the 51.8 m BPC)? The dimensions of the pillar and the entries were obtained from an AutoCAD map of Mine A, then rounded to the nearest even whole number. The stratigraphic sequence in the model was based on the Australian longwall case study discussed in section 4.4.2, as no core data was available for Mine A at the instrumented location.

It should be noted that due a lack of relevant geological and geotechnical data from Mine A, the model developed and discussed herein is schematic in nature, and no attempt was made to quantitatively match the field measured stress profiles. All rock layers were

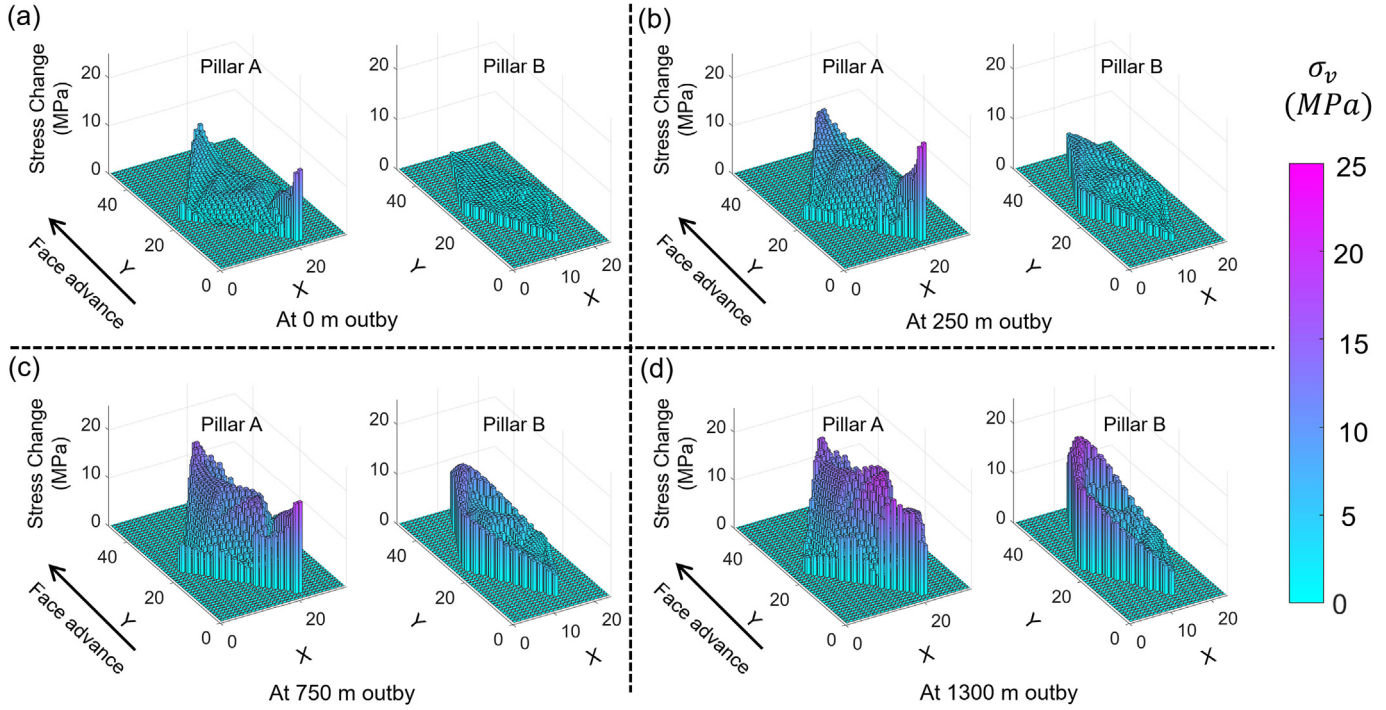

Fig. 11. Two dimensional stress distribution in Chain Pillar A and B for longwall face location of (a) 0 m outby, (b) 250 m outby, (c) 750 m outby, and, (d) 1300 m outby.

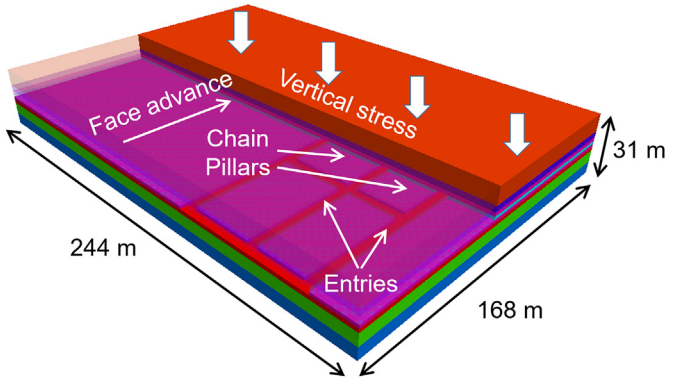

Fig. 12. Overall geometry of the hypothetical longwall model.

Table 4
Thickness and rockmass elastic parameters for different layers in model.[47]

Layer	Thickness (m)	Rockmass Young's Modulus (GPa)	Rockmass Poisson's ratio
Interbedded sandstone (roof)	9.2	12.0	0.26
Mudstone (roof)	4.8	10.0	0.26
Coal	2.8	3.0	0.25
Mudstone (floor)	2.0	12.0	0.26
Interbedded sandstone (floor)	6.0	12.0	0.26
Sandstone (floor)	6.0	15.0	0.26

represented by an isotropic elastic constitutive model with parameters listed in Table 4[47] A vertical stress corresponding to 236.5 m of overburden was applied to the top of the model, and the body stress for coal seam and 14 m of overburden was considered by setting the acceleration due to gravity at 9.81 m/s^2. Roller constraints were assigned to the bottom and sides of the FLAC^{3D} model.

The model behavior is expected to be influenced by the load carrying capacity of the gob, which required an explicit consideration of the gob loading mechanism within the model. A methodology similar to Esterhuizen et al.[18] was followed, whereby the excavated coal was replaced by an equivalent gob material that exhibits a hyperbolic hardening behavior.[54] The modulus of the gob material was varied per[54]

$$\sigma = \frac{a\,\varepsilon}{b-\varepsilon}$$
$$E = \frac{d\sigma}{d\varepsilon} = ab/(b-\varepsilon)^2 \quad (14)$$

where σ is the stress, ε is the strain, and a and b are two constants that were found to be 7.65 MPa and 0.442 for shales and 13.03 MPa and 0.427 for sandstones.[55] Esterhuizen et al.[18] tabulated the gob parameters 'a' and 'b' for four different overburden types. Since the different rock layers were modeled as elastic material, the roof deformation after mining was significantly lower than would be expected in reality, meaning much lower 'a' and 'b' parameter values had to be used for the gob to develop any appreciable stiffness in the model. A FISH function was called every 500 solution steps that modified the Young's modulus of the gob according to Eq. (14). With a = 5.9 MPa and b = 0.05, the gob achieved pre-mining vertical stress at a distance of ~55 m from the longwall face, similar to what was obtained by Abbasi et al.[51] in modeling a longwall mine in Illinois. While it is not known whether the gob compacted completely within 55 m for Mine A, this was assumed in order to obtain realistic gob parameters. The longwall face was advanced in two 40 m steps whereby the coal elements were first replaced by the elastic gob elements and then solved until mechanical equilibrium was achieved.

In practice, shield supports are used along the length of the longwall face to ensure safe extraction of the coal. Within the first few meters of the face, the coal is generally yielded,[56] lowering its effective stiffness. The powered shield support, being stiffer in comparison to the yielded coal, therefore should transfer a large proportion of the nearby in-situ load from the overburden to the floor. A consequence of this phenomenon is the reduction in the distance ahead of (outby) the face that experiences change in stress levels. The shield load transfer mechanism was simulated in the elastic model by replacing the first 4 m of the

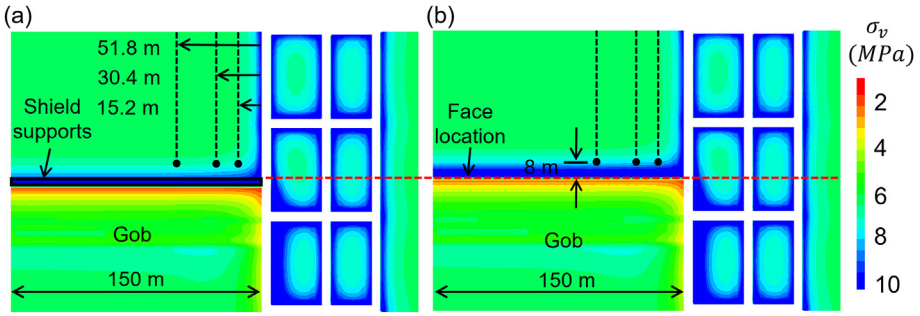

Fig. 13. Vertical stress contour at mid-height of the coal seam (a) with shield support, and, (b) without shield support.

excavated material by a material that was three times stiffer than the coal mass.

Fig. 13 shows the vertical stress contour along the mid-height of the longwall panel with and without consideration of shield supports. The stress monitoring points and the profile locations (as in Fig. 10) are also shown by black circles and black discontinuous lines, respectively. It can be seen that all the measurement points experienced significantly lower stresses when the shield supports were considered in the model. This explains why the 51.8 m BPC experienced negligible change in stress when the extent of the roof between the compacted gob and the shield supports was left unsupported. The weight of this unsupported region was ultimately borne by the shield supports, compacted gob and the first 8 m of the coal face.

Although subtle in the presented results (refer to the stress level at the monitoring points in Fig. 13), profiles drawn at 8 m from the face showed an exponential decay in stress from the edge of the panel inwards. This explains the trend in data shown in Fig. 10 and is consistent with the hypothesized stress transfer mechanisms. In order to understand why such a behavior was exhibited by the model, the modulus distribution of the gob material was analyzed. It was found that along the edge of the panel, the gob had a lower modulus and consequently carried a lesser proportion of the overburden load. As discussed before, this is caused by the flexural resistance of the pillar-supported roof layers that prevent complete compaction of the gob material at the panel edge.

6. Discussion

Abutment angles around the globe have been found to vary between 6°-27°[24] with 21° being used as a conservative estimate for most US coal mines.[3] Other studies have found the abutment angle to decrease with increase in mining depth beyond 274 m.[33] For Mine A, the depth is around 250 m, and therefore might be expected to correspond to an abutment angle of roughly 21°. However, the values calculated from BPC measurements are significantly lower than this abutment angle. Relatively low values in the range of 5° - 15° were also reported by Hill et al.[24] for Western US mines. A possible explanation is that the traditional abutment angle model may be overestimating the magnitude of abutment load for Western US mines, indicating that a larger than typical amount of load is transferred elsewhere (for example, to the gob) due to different caving characteristics.

An interesting observation made during the BPC data analysis is the simultaneous loss of load-carrying capacity of instrument 6B and Array 7 when the longwall face reached 228 m outby. It seems that instead of a progressive expansion of the damage zone as was proposed by Mark,[3] fracturing initiated in discrete episodes over thick sections of the pillar. The authors have not previously observed such episodial-type behavior; if indeed this phenomenon is real, further study is required to understand the governing mechanics. It is possible that fracturing initiated in Array 7 first and then progressed to 6B, but this might have been masked by the limited temporal resolution of the dataset. In any case, for the purposes of analyses in this paper, it was assumed that the entire 13.7 m of the rib yielded when the face reached 228 m outby.

Based on an understanding of coal damage mechanics, one would expect the yield strengths to be similar at equal distances from the pillar edge. However, it was found that the yield strength along the shorter edge was higher than those along the longer edge of the pillar (i.e. using BPC Array 7 and instrument 6B). The exact cause for this behavior is not immediately apparent and is difficult to explain. Because this trend was observed along all of the pillar edges, the likelihood of the data being faulty is thought to be extremely low. One possible reason for this unexpected behavior is damage induced in the rib due to the rapid unloading 10 m after the face went past the instrumented location (refer Fig. 4a). It is important to reiterate here that this loading-unloading cycle was only observed in BPC Array 7 and instrument 6B. To date, no study has been conducted to understand the effect of this load cycle on the integrity of the coal rib. In addition to the moment applied by the flexure of the immediate roof on the coal rib (which opens the cleat planes along the roof), the authors believe that the loading-unloading cycle may have damaged the first 13 m of the rib.

A second possible reason for this behavior could be the effect of cleat orientation on coal strength. The cleats at Mine A are near-vertical and trend approximately NE-SW. The panel, on the other hand, is oriented North-South which renders either edge of the pillar equally vulnerable to damage formation along cleats. With the panel currently inaccessible for further inspection, it is unclear whether there was any local variation in the cleat angle. If the cleats were trending closer to N, then the likelihood of spalling would be higher along the entry side of the pillar. Along the shorter edge, spalling would be constrained in the lateral direction, forcing fractures to propagate through intact coal.

Evidence of strength anisotropy in coal due to cleat orientation was found by Kim et al.[57] and Song et al.[58] during laboratory testing. Under actual field conditions, cracks can propagate rather freely along the pillar periphery.[59] As discussed by Diederichs,[59] the crack propagation mechanism is highly sensitive to confinement levels and a small increase in confinement can suppress the spalling mechanism. The confining stress generated across cleat planes on adjacent pillar faces in Mine A could possibly explain the stark difference in the observed stress levels.

It is useful to note here that the intersection of Bieniawksi's[1] stress gradient curve and the Mark and Iannacchione[21] average stress gradient curve (derived from field measurements) lies at x (distance into pillar)/h (height of pillar) = 0.18 (Fig. 14), which gives x = 0.52 m for Mine A. Beyond the intersection point, the average stress lies above the Bieniawski's[1] curve.[21] For Mine A, the damage due to the loading-unloading cycle or local variability in the cleat angle might have lowered the actual yield strength at x = 2.52 m (used for calculating CF_{7B}) such that it matched the strength predicted by the Bieniawksi's[1] curve. This implies that the actual (undamaged) stress gradient in the pillars is higher than Bieniawski's[1] curve would suggest.

Besides BPC array 7 and instrument 6B, the only other data point that exhibited yielding was 1A, located 1.72 m from the shorter edge of Pillar A. The yield strength at this point was estimated to be 24.9 MPa, which is approximately double of what is predicted by Bieniawksi's[1]

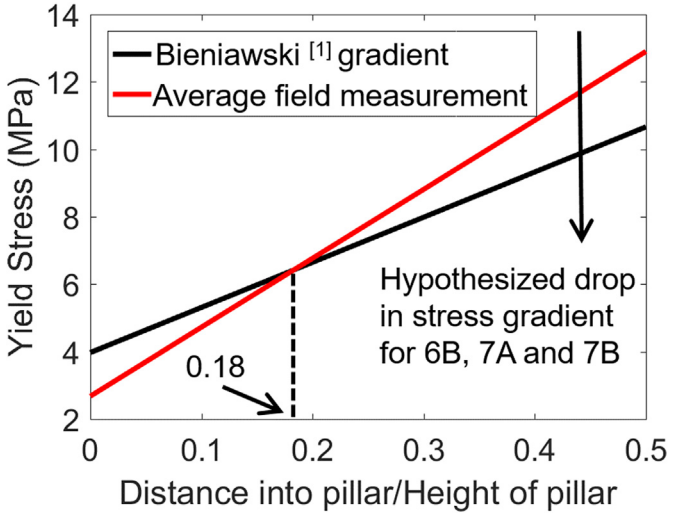

Fig. 14. Plot of average field measured stress gradient[21] and Bieniawksi's[1] stress gradient.

gradient equation. Clearly, the yield strengths are underestimated for points located deeper within the pillar. The use of Bieniawksi's[1] gradient equation should, therefore, be restricted to within $x/h < \sim 0.2$ from the rib. While the gradient approach for calculating a conversion factor was successful in this case, it might not yield reasonable values under every condition. Where possible, the appropriateness of the conversion factor should be validated using a secondary approach, as was done in this study.

7. Conclusions

This study has presented an extensive suite of borehole pressure cell data from a Western US mine with the goal of advancing our knowledge of the stress redistribution process in longwall chain pillars. A new method was employed for converting the raw data into actual stresses experienced by the host rock. Although this method worked well for Mine A, care should be exercised when applying it to other geo-mining conditions.

The abutment angle and the front abutment factor at Mine A were found to be significantly lower than what is normally associated with US longwall mines. The low abutment angle of the order of 11° was verified using the BPC measurements taken in the solid coal ahead of (outby) the longwall face. The stress rise in the yield zone was found to be bi-linear in nature which agreed with a calibrated mine model (from a case study in Australia) recently developed by the authors.

Some other trends such as a drop in stress from the edge of the panel towards the center and negligible stress change about 51 m into the solid coal face were also observed. Using an elastic FLAC^{3D} model with appropriate consideration of gob loading and face shield supports, these observations could be explained. Finally, the global stress redistribution process was presented in three dimensions using 3D bar charts for different locations of the longwall face.

Understanding the stress transfer process along with the local damage progression in the entry side rib will ultimately help the mining industry in better assessing pillar stability and improving the methodology that currently exists for determining pillar dimensions. The results suggest that using the current design approach ($\beta = 21°$) without a proper estimation of abutment angle might lead to highly over designed coal pillars.

Conflicts of interest

There is no conflict of interest in preparation of this paper.

Acknowledgements

The authors would like to extend their sincere gratitude to NIOSH for the financial support. Special thanks to Dr. Mark Larson, Dr. Bo-Hyun Kim and Rami Abousleiman for reviewing the manuscript and providing critical suggestions. The research conducted for this study was funded by the National Institute for Occupational Safety and Health (NIOSH) under Grant Number 200-2016-90154.

Appendix A. Supplementary data

Supplementary data to this article can be found online at https://doi.org/10.1016/j.ijrmms.2019.06.008.

References

1. Bieniawski ZT. *Rock Mechanics Design in Mining and Tunneling.* Rotterdam: Balkema; 1984.
2. Peng SS, Chiang HS. *Longwall Mining.* New York: Wiley; 1984.
3. Mark C. *Analysis of Longwall Pillar Stability* Ph.D. Dissertation The Pennsylvania State University; 1987.
4. King HJ, Whittaker BN. A review of current knowledge on roadway behaviour. *Proc Symp Roadway Strata Control.* 1971:73–87.
5. Wilson AH. An hypothesis concerning pillar stability. *Min Eng.* 1972;131:409–417.
6. Schuerger MG. An investigation of longwall pillar stress history. *Proceedings of the 4th Conference on Ground Control in Mining, Morgantown.* 1985; 1985:41–49.
7. Allwes RA, Listak JM, Chekan GJ, Babich DR. The effects of a retreating longwall on a three-entry gate road system. *USBM RI.* 1985;8966:19.
8. Lu PH. Ground control study of a mechanized longwall coal operation in West Virginia. *ISBM RI.* 1985;8929:34.
9. Carr F, Wilson AH. A new approach to the design of multi-entry developments for retreat longwall mining. *Proceedings of 2nd Conference on Ground Control in Mining, Morgantown.* 1982; 1982:1–22.
10. Choi DS, McCain DL. Design of longwall systems. *Trans AIME-SME.* 1980;258:1761–1764.
11. Hsuing SM, Peng SS. Chain pillar design for U.S. longwall panels. *Min Sci Technol.* 1985;2:279–305.
12. Larson MK, Whyatt JK. Panel-scale modeling of a deep longwall panel: The MULSIM alternative. *Proceedings of the 32nd International Conference on Ground Control in Mining, Morgantown, West Virginia.* 2013; 2013.
13. Tulu IB, Esterhuizen GS, Gearhart D, Klemetti TM, Mohamed KM, Su DWH. Analysis of global and local stress changes in a longwall gateroad. *Int J Min Sci Technol.* 2018;28(1):127–135.
14. Mark C. Coal bursts in deep longwall mines of the United States. *Int J Coal Sci Technol.* 2016;3(1):1–9.
15. Rezaei M, Farouq Hossaini M, Majdi A. Determination of longwall mining-induced stress using the strain energy method. *Rock Mech Rock Eng.* 2015;48:2421–2433.
16. Rezaei M, Farouq Hossaini M, Majdi A. Development of a time-dependent energy model to calculate the mining-induced stress over gates and pillars. *J Rock Mech Geotech Eng.* 2015;7(3):306–317.
17. Salamon MDG. Energy considerations in rock mechanics: Fundamental results. *J S Afr Inst Min Metall.* 1984;84(8):233–246.
18. Esterhuizen E, Mark C, Murphy MM. Numerical model calibration for simulation coal pillars, gob and overburden response. *Proc 29th Int Conf Gr Control Min, Morgantown, WV.* 2010:46–57.
19. Yasitli Ne, Unver B. 3D numerical modeling of longwall mining with top-coal caving. *Int J Rock Mech Min Sci.* 2005;42:219–235.
20. Zhang G, Liang S, Tan Y, Xie F, Chen S, Jia H. Numerical modeling for longwall pillar design: A case study from a typical longwall panel in China. *J Geophys Eng.* 2015;15:121–134.
21. Mark C, Iannacchione AT. Coal pillar mechanics: Theoretical models and field measurements compared. *Proceedings of the Workshop on Coal Pillar Mechanics and Design. Pittsburgh, PA: U.S. Department of the Interior, Bureau of Mines, IC.* vol. 9315. 1992; 1992:78–93.
22. Colwell M, Frith R, Mark C. Analysis of Longwall Tailgate Serviceability (ALTS): A chain pillar design methodology for Australian conditions. *Proceedings of the Second International Workshop on Coal Pillar Mechanics and Design, NIOSH: IC.* vol. 9448. 1999; 1999:33–48.
23. Larson MK, Whyatt JK. Load transfer distance calibration of a coal panel scale model: A case study. *Proceedings of the 31st International Conference on Ground Control in Mining, Morgantown, WV.* 2012; 2012:11.
24. Hill D, Stone R, Suchowerska A, Trueman R. Pillar abutment loading- new concepts for coal mining industry. *Proceedings of 15th Coal Operator's Conference, University of Wollongong, Australia.* 2015; 2015:204–211.
25. Friedel MJ, Jackson MJ, Williams EM, Olson MS, Westman E. Tomographic imaging of coal pillar conditions: Observations and Implications. *Int J Rock Mech Min Sci Geomech Abstr.* 1996;33(3):279–290.
26. Luxbacher K, Westman E, Swanson P, Karfakis M. Three-dimensional time-lapse velocity tomography of an underground longwall panel. *Int J Rock Mech Min Sci.* 2008;45:478–485.
27. Hosseini N, Oraee K, Shahriar K, Goshtasbi K. Studying the stress redistribution

around the longwall mining panel using passive seismic velocity tomography and geostatistical estimation. *Arab J Geosci.* 2013;6:1407–1416.
28. Cai W, Dou L, Cao A, Gong S, Li Z. Application of seismic velocity tomography in underground coal mines: A case study of Yima mining area, Henan, China. *J Appl Geophys.* 2014;109:140–149.
29. Wilson AH. The stability of underground workings in the soft rocks of the coal measures. *Int J Min Eng.* 1983;1:91–187.
30. ISRM Suggested Methods. Brown ET, ed. *Rock Characterization Testing and Monitoring.* Oxford: Pergamon; 1981 1981: 113 – 116 and 123 – 127.
31. Heasley KA, Saperstein LW. Practical subsidence prediction for the operating coal mine. *Proceedings of the 2nd Workshop on Surface Subsidence Due to Underground Mining, West Virginia University, Morgantown, West Virginia.* 1986; 1986:54–67.
32. Colwell M. The abutment angle model and its appropriate use for longwall tailgate design. *Proceedings of the 18th Coal Operators' Conference, Mining Engineering, University of Wollongong.* 2018; 2018:152–164.
33. Tulu IB, Heasley KA. Investigating the mechanics of pillar loading through the analysis of in-situ stress measurements. *Proceedings of the 45th US Rock Mechanics/Geomechanics Symposium, San Francisco, CA.* 2011; 2011.
34. Lawson HE, Whyatt J, Larson MK. Investigation of pillar loading considerations in determination of pillar stability factors for longwall gateroad design. *Proceedings of the 32nd International Conference on Ground Control in Mining, Morgantown, West Virginia.* 2013; 2013.
35. Larson MK, Lawson HE, Tesarik DR. Load transfer distance measurements at two mines in the Western US. *Proceedings of the 34nd International Conference on Ground Control in Mining, Morgantown, West Virginia.* 2015; 2015.
36. Wagner H. Determination of the complete load-deformation characteristics of coal pillars. *Proceedings of the 3rd International Congress Rock Mechanics, Washington, DC.* 1974; 1974:1076–1081.
37. Braden B. The surveyor's area formula. *Coll Math J.* 1986;17(4):326–337.
38. Babcock CO. Equations for the analysis of borehole pressure cell data. *Proceedings of the 27th U.S. Symposium on Rock Mechanics, University of Alabama, Tuscaloosa, AL.* 1980; 1980:512–519.
39. Heasley KA. Understanding the hydraulic pressure cell. *Proceedings of the 30th U.S. Symposium on Rock Mechanics, Morgantown, WV.* 1989; 1989:485–492.
40. Lu PH. Mining-induced stress measurements with hydraulic borehole pressure cells. *Proceedings of the 25th U.S. Symposium on Rock Mechanics, Northwest. University, Evanston, IL.* 1984; 1984:204–211.
41. Mohamed KM, Tulu IB, Murphy MM. Numerical model calibration for simulating coal ribs. *Proceedings of the Society for Mining, Metallurgy and Exploration Inc Annual Conference, Pheonix, Arizona.* 2016; 2016.
42. Mark C, Barton TM. Pillar design and coal strength. *Proc New Technol Gr Control Retreat Min, NIOSH IC.* 1997;9446:49–59.
43. Agioutantis Z, Karmis M. *Surface Deformation Prediction System for Windows.* Virginia Polytechnic Institute and State University; 2009.
44. Mukherjee C, Sheorey PR, Sharma KG. Numerical simulation of caved goaf behavior in longwall workings. *Int J Rock Mech Min Sci Geomech Abstr.* 1994;31(1):35–45.
45. Suchowerska AM, Merifield RS, Carter JP. Vertical stress changes in multi-seam mining under supercritical longwall panels. *Int J Rock Mech Min Sci.* 2013;61:306–320.
46. Colwell MG. *A Study of the Mechanics of Coal Mine Rib Deformation and Rib Support as a Basis for Engineering Design* Ph.D. thesis Australia: University of Queensland; 2006.
47. Sinha S, Walton G. Modeling the Behavior of a Coal Pillar Rib Using the Progressive S-Shaped Yield Criterion. *J Rock Mech Geotech Engr.* 2019 submitted.
48. Oyanguren PR. Simultaneous extraction of two potash beds in close proximity. *Proceedings of the 5th International Strata Control Conference.* 1972; 1972:5.
49. Wade LV, Conroy PJ. Rock mechanics study of a longwall panel. *Min Eng.* 1980;268:1728–1734.
50. Campoli AA, Barton TM, Dyke F, Gauna M. *Gob and Gate Road Reaction to Longwall Mining in Bump-Prone Strata.* Bureau of Mines, RI 9445; 1993:48.
51. Abbasi B, Chugh YP, Gurley H. An analysis of the possible fault displacements associated with a retreating longwall face in Illinois. *Proceedings of 48th U.S. Rock Mechanics/Geomechanics Symposium, MN, USA.* 2014; 2014.
52. Li W, Bai J, Peng S, Wang X, Xu Y. Numerical modeling for yield pillar design: A case study. *Rock Mech Rock Eng.* 2015;48:305–318.
53. Itasca. *FLAC 3D Version 5.0: Theory and Background.* Minneapolis, Minnesota: Itasca Consulting Group; 2016.
54. Salamon MDG. Mechanism of caving in longwall coal mining. *Proceedings of the 31st US Rock Mechanics Symposium, Denver, Colorado, USA.* 1990; 1990:161–168.
55. Pappas DM, Mark C. *Behavior of Simulated Gob Material.* U.S. Bureau of Mines RI 9458; 1993.
56. Song G, Chugh YP, Wang J. A numerical modelling study of longwall face stability in mining thick coal seams in China. *Int J Min Miner Eng.* 2017;8(1):35–55.
57. Kim B, Walton G, Larson MK, Berry S. Experimental study of the confinement-dependent characteristics of a Utah coal considering the anisotropy of cleats. *Int J Rock Mech Min Sci.* 2018;105:182–191.
58. Song H, Jiang Y, Elsworth D, Zhao Y, Wang J, Liu B. Scale effects and strength anisotropy in coal. *Int J Coal Geol.* 2018;195:37–46.
59. Diederichs MS. The 2003 geotechnical colloquium: Mechanistic interpretation and practical application of damage and spalling prediction criteria for deep tunnelling. *Can Geotech J.* 2007;44:1082–1116.